

# Fundamental properties, localization threshold, and the Tomonaga–Luttinger behavior of electrons in nanochains

Adam Rycerz and Jozef Spałek

Marian Smoluchowski Institute of Physics,  
 Jagiellonian University, Reymonta 4, 30-059 Kraków, Poland,  
 e-mail: adamr@th.if.uj.edu.pl, ufspalek@if.uj.edu.pl

the date of receipt and acceptance should be inserted later

**Abstract.** We provide a fairly complete discussion of the electronic properties of nanochains by modelling the simplest quantum nanowires within a recently proposed approach which combines the *Exact Diagonalization* in the Fock space with *Ab Initio* calculations (EDABI method). In particular, the microscopic parameters of the second-quantized Hamiltonian are determined, and the evolution of the system properties is traced in a systematic manner as a function of the interatomic distance (the lattice parameter,  $R$ ). Both the many-particle ground state and the dynamical correlation functions are discussed within a single scheme. The principal physical results show: (i) the evolution of the electron momentum distribution and its analysis in terms of the Tomonaga–Luttinger scaling, (ii) the appearance of mixed metallic and insulating features (*partial localization*) for the *half-filled* band case, (iii) the appearance of a universal *renormalized* dispersion relation for the electron energy, which incorporates both the band-structure and the Hubbard-splitting features in the presence of electron interactions, and (iv) the transformation from a *highly-conducting* nanometallic state to the *charge-ordered* nanoinsulator in the quarter-filled case. The analysis is performed using the Wannier functions composed of an adjustable Gaussian  $1s$ -like basis set, as well as includes a *long-range* part of the Coulomb interaction.

**PACS.** 73.63.-b Electronic transport in nanoscale materials and structures – 31.15.Ar Ab initio calculations – 71.10.Hf Lattice fermion models – 71.27.+a Strongly correlated electron systems

## 1 Introduction

Recent developments in computational as well as analytical methods have lead to a successful determination of the electronic properties of semiconductors and metals starting from LDA [1], LDA+U [2], and related [3] approaches. Even strongly correlated systems, such as  $V_2O_3$  (which undergoes the Mott transition) and high-temperature superconductors have been treated in this manner [4]. However, the discussion of the metal–insulator transition of the Mott–Hubbard type is not yet possible in a systematic manner, particularly for low-dimensional systems. These difficulties are caused by the circumstance where the electron–electron interaction is comparable, if not stronger, than the single-particle energy. In effect, the procedure starting from the single-particle picture (band structure) and subsequently including the interaction via a *local* potential, may not be appropriate. In such situations, one resorts to parametrized models of correlated electrons, where the single-particle and the interaction-induced aspects of the electronic states are treated on equal footing. The single-particle wave-functions are contained in the formal expressions of the model parameters. We have pro-

posed [5] to combine the two efforts in an exact manner, at least for small systems.

In our method of approach (EDABI), we *first* rigorously determine the ground-state energy  $E_G$  of the system of interacting particles using the occupation-number representation, which is expressed as a function of the microscopic parameters. *Second*, we optimize this energy with respect to the wave-functions contained in these parameters by deriving the *self-adjusted wave equation* for them. Physically, the last step amounts to allowing the single-particle wave functions to relax in the correlated state. In practice, we propose the particular class of those functions, which are obtained by minimizing variationally the ground-state energy  $E_G$  with respect to their size (effective Bohr radius). In brief, our method of solution does not limit itself to an exact diagonalization of the parametrized Hamiltonian, but also involves an adjustment of the single-particle wave function to obtain a true ground state of a correlated quantum many-body system.

The EDABI method has been overviewed in a number of papers [6,7,8], so here we concentrate on its application to one-dimensional (1D) nanochains of  $N \leq 16$  atoms, close to the metal–insulator crossover transition. This paper complements our recent study of such sys-

tems [6,7] with the systematic analysis of both *half-* and *quarter-filled* band cases, as well as with the analysis of its transport properties. Throughout the paper we use the adjustable Wannier functions composed of a Gaussian basis set (STO–3G), which are determined explicitly from minimization of the system ground–state energy  $E_G$  as a function of the interatomic distance  $R$ .

The question of delocalization of atomic states also has practical relevance. Namely, in dealing with electronic properties of quantum dots one usually *assumes* the existence of the effective–mass states. Whether this assumption is well founded for particular systems can only be determined by finding the critical interatomic distance, above which the states are localized. In this context, we find such critical distance for model systems composed of *s*-like states.

The structure of the paper is as follows. In Section 2 we briefly present the basic idea of the EDABI method. Then, in Section 3, we provide the numerical ground–state analysis of nanochains with the long–range Coulomb interaction. Namely, we first discuss the electron momentum statistical distribution function for the half–filled case and analyse it in terms of Tomonaga–Luttinger scaling (including the logarithmic correction, *cf.* Section 3.1) and illustrate the charge–density wave ordering for the quarter filling (*cf.* Section 3.2), as well as the analysis the  $N$ -particle wave function localization according to the method developed by Resta [9]. In Section 4, we calculate the system charge and spin gaps, as well as perform the finite–size scaling with  $1/N \rightarrow 0$  on these quantities. We also analyze the spectral density and extract from it the *renormalized* dispersion relation for the interacting electrons in a nanochain. To the best of our knowledge, such an exact renormalized one–electron *band structure* has not been determined before. Finally, the application of the present scheme to the higher (*ns*-like) valence orbital systems would make possible a direct comparison with the experimental results for quantum nanowires made of noble and alkaline elements. Also, the correspondence between the localization criteria inferred from the ground–state properties on one side, and from the dynamical correlation functions on the other, is established.

## 2 The combined exact diagonalization ab–initio (EDABI) method

The basic idea of the EDABI method [5,8] is illustrated on the block diagram exhibited in Fig. 1. We start from choosing the initial Wannier basis set  $\{w_i(\mathbf{r})\}$ , composed of atomic–like wave functions (here a trial Gaussian basis set) with radii  $a_i$ . Next, we write down the system Hamiltonian in the second–quantization form and determine the ground–state energy  $E_G$  together with the corresponding state in the Fock space  $|\Psi_0\rangle$  by employing the Lanczos procedure, for example. Then, the Wannier basis set  $\{w_i(\mathbf{r})\}$  is optimized with respect to the atomic radii  $a_i$ , contained in the atomic wave functions (here represented by Gaussians) composing  $w_i(\mathbf{r})$ , until the minimal ground–state

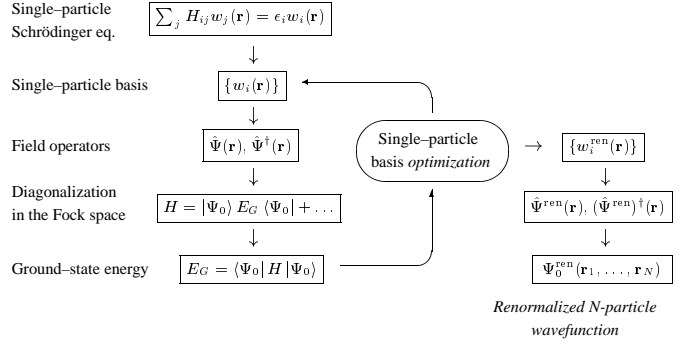


**Fig. 1.** Flowchart diagram of the EDABI method. The part on the far right provides *renormalized* Wannier functions, field operators, and  $N$ -particle wave function. The top line is absent if we select the trial Wannier functions as composed of adjustable Gaussian orbitals (e.g. the STO–3G basis).

energy  $E_G$  is reached [5] for a given lattice parameter  $R$ . On the right, we list the renormalized quantities (for the optimized basis), which can be calculated once the whole two–step procedure has provided convergent results.

## 3 The correlated electrons in a nanochain

We consider the system of  $N_e$  electrons on  $N$  lattice sites arranged periodically, each site containing a single valence orbital and an infinite–mass ion (i.e. we start from hydrogenic–like atoms). The Hamiltonian, including *all* the direct Coulomb–interaction terms and neglecting other (e.g. exchange terms), can be written down (up to a constant) in the form

$$H = \epsilon_a^{\text{eff}} \sum_i n_i + t \sum_{i\sigma} \left( a_{i\sigma}^\dagger a_{i+1\sigma} + \text{HC} \right) + U \sum_i n_{i\uparrow} n_{i\downarrow} + \sum_{i<j} K_{ij} \delta n_i \delta n_j, \quad (1)$$

where  $\delta n_i \equiv n_i - 1$ ,  $\epsilon_a^{\text{eff}} = \epsilon_a + N^{-1} \sum_{i<j} (2/R_{ij} + K_{ij})$  (in Ry) is the effective atomic level,  $R_{ij}$  is the distance between the  $i$ -th and  $j$ -th atoms,  $t \equiv \langle w_i | T | w_{i+1} \rangle$  is the nearest–neighbor hopping,  $U \equiv \langle w_i w_i | V | w_i w_i \rangle$  and  $K_{ij} \equiv \langle w_i w_j | V | w_i w_j \rangle$  are the intra– and inter–site Coulomb repulsions, respectively. In the present form of the Hamiltonian, all the *mean–field* Coulomb terms are collected in  $\epsilon_a^{\text{eff}}$ , whereas the last term represents the *correlation part* of the long–range Coulomb interaction. We shall test *a posteriori* whether the tight–binding approximation for the hopping term is valid. Also, the effect of the direct (Heisenberg) exchange is negligible, since the kinetic exchange term will always be dominant [7]. The microscopic parameters are expressed in terms of the Wannier functions  $\{w_i(\mathbf{r})\}$  composed of Gaussian–type orbitals.

The Hamiltonian (1) is diagonalized in the Fock space with the help of Lanczos technique. As the microscopic parameters  $\epsilon_a^{\text{eff}}$ ,  $t$ ,  $U$ , and  $K_{ij}$  are calculated numerically in the Gaussian basis, the orbital size of the  $1s$ -like state

expressed in this basis is subsequently adjusted to obtain the minimal ground–state energy  $E_G$ , as a function of the interatomic distance  $R$ . Earlier, we have shown [5] that such a combined exact diagonalization – *ab initio* study of the one dimensional system provides the localization threshold, the electron–lattice couplings, and the dimerization magnitude. Moreover, the utilization of the Gaussian–type orbitals leads to a variational procedure that converges rapidly with the lattice size  $N$  [7,10]. In effect, one can extrapolate the optimal orbital parameters for larger  $N$  using those obtained for small systems (i.e. for  $N = 6 \div 10$ ), which speeds up the computation remarkably. The purpose of this paper is to discuss basic solid–state properties of the nanoscopic systems *per se*, and (in some instances) their infinite correspondants by performing the finite–size scaling.

### 3.1 Statistical distribution and the Tomonaga–Luttinger scaling: The half–filled case

We now discuss the electron momentum distribution of 1D chain of  $N = 6 \div 16$  atoms to address the question of whether the system composes either a *Luttinger–liquid* or forms an insulating (Mott–Hubbard) state. We first summarize, following Voit [11], the properties of 1D conductors, which include the two principal characteristics:

- (i) A continuous momentum distribution function, showing a singularity near the Fermi level  $k \rightarrow k_F$  of the form (Solyom, Ref. [11])

$$n_{k\sigma} = n_F + A |k_F - k|^\theta \operatorname{sgn}(k_F - k), \quad (2)$$

where  $\theta$  is a non–universal (*interaction–dependent*) exponent; in consequence, it leads to the absence of fermionic quasi–particles (the quasi–particle residue in vanishes as  $z_k \sim |k_F - k|^\theta$  when  $k \rightarrow k_F$ ). In other words, the *Fermi ridge* is absent in this case.

- (ii) Similar power–law behavior of all the other physical properties, particularly of the single–particle density of states,  $\mathcal{N}(\omega) \sim |\omega - \mu|^\theta$  (i.e. a presence of a *pseudogap*), that implies a Drude weight  $D > 0$  for  $\theta < 1$ .

In the case of lattice models, such as the (*extended*) Hubbard model, the Luttinger liquid behavior is predicted by the renormalization group (RG) mapping onto the Tomonaga–Luttinger model [11]. Through such mapping, one can also expect, with the increasing  $N$ , a gradual convergence of the discrete momentum distribution  $n_{k\sigma}$  into the continuous power–law form (2). This hypothesis was first checked numerically for the Hubbard model by Sorella *et al.* [12].

Here we present the approach to a finite 1D chain with a long–range Coulomb interaction, as described by the Hamiltonian (1), with a simultaneous evaluation of the model parameters by optimizing the single–particle wave functions contained in those parameters [5]. The values of the parameters in the ground state are shown in Table 1 as a function of the interatomic spacing (all quantities are in atomic units). Only the value  $K_1$  of the

**Table 1.** Microscopic parameters (in Ry) of Hamiltonian (1) for a nanochain calculated in the adjusted STO–3G basis composing the Wannier functions. The numerical extrapolation with  $N \rightarrow \infty$  is performed. The values of the inverse orbital size  $\alpha_{\min}$  (in the units of the Bohr radius  $a_0$ ) and of the ground–state energy  $E_G/N$  (for  $N = 10$ ), are also provided.

$R/a_0$	$\alpha_{\min}a_0$	$\epsilon_a^{\text{eff}}$	$t$	$U$	$K_1$	$E_G/N$
1.5	1.363	0.100	-0.831	2.054	1.165	-0.749
2.0	1.220	-0.550	-0.442	1.733	0.911	-0.930
2.5	1.122	-0.797	-0.264	1.531	0.750	-0.979
3.0	1.062	-0.902	-0.171	1.407	0.639	-0.991
4.0	1.013	-0.971	-0.080	1.291	0.493	-0.992
5.0	1.004	-0.987	-0.037	1.258	0.399	-0.992

intersite Coulomb interaction  $K_{ij} \equiv K_{|i-j|}$  for nearest neighbors is listed, since more distant interactions scale essentially in the same manner as their classical values,  $K_{ij} \approx 2/|\mathbf{R}_i - \mathbf{R}_j|$ . One should also note that the orbital size  $\alpha^{-1}$  renormalized by the electron–electron interaction is about 30 – 40% smaller in the correlated state than the corresponding value in the atomic limit ( $\alpha^{-1} = a_0$ ). Therefore, the tight–binding approximation made for the hopping term in Eq. (1) is applicable to a good accuracy even for the lattice constant  $R/a_0 = 2.0$ , but not much below this value.

The discrete electron–momentum distribution for the half–filling ( $N_e = N$ ) is depicted in Fig. 2a, while in Fig. 2b we replot it on a *log–log* scale together with the fitted theoretical curves, as explained below. In order to obtain these results, we use the boundary conditions (BC) that minimize the ground–state energy for a given  $N$  (namely, the *periodic* BC for  $N = 4n + 2$  atoms and the *antiperiodic* BC for  $N = 4n$ , at the half–filling). A systematic arrangement of the distribution–function data in Fig. 2a for different  $N$  values is striking, in that for smaller  $R$  it is *Fermi–like*.

To extract the Luttinger–liquid exponent  $\theta$  accurately from the data for finite  $N$ , it was necessary to also include the higher scaling corrections to (2). They can be obtained from the Tomonaga mapping in the form of an expansion in the powers of  $\ln(\pi/|k_F - k|R)$ , namely,

$$\ln |n_F - n_{k\sigma}| = -\theta \ln z + b \ln \ln z + c + \mathcal{O}(1/\ln z), \quad (3)$$

where  $z \equiv \pi/|k_F - k|R$ . This singular form of the expansion is required by the especially slow approach to the RG fixed point (Solyom, Ref. [11]). Obviously, by neglecting the logarithmic corrections one reaches the asymptotic form (2) for  $k \approx k_F$ . The solid lines in Fig. 2b represent the formula (3); the fitted values of the parameters  $\theta$ ,  $b$ , and  $c$  are also listed in Table 2. The quality of the fit is decisively worse for points far away from the Fermi momentum, and depends on  $N$  since the Fermi wave vector is  $N$ –dependent, i.e.  $k_F^N = k_F^\infty(1 - 2/N)$ , where  $k_F^\infty = \pi/(2R)$  represents the Fermi wave vector in the  $N \rightarrow \infty$  limit. The exponent  $\theta$  is also plotted in Fig. 2c as a function of the lattice parameter  $R$  showing that it crosses the critical value  $\theta = 1$  (corresponding to the metal–insulator boundary in 1D) for  $R_c = 2.60a_0$  ( $a_0 = 0.529 \text{ \AA}$  is the Bohr

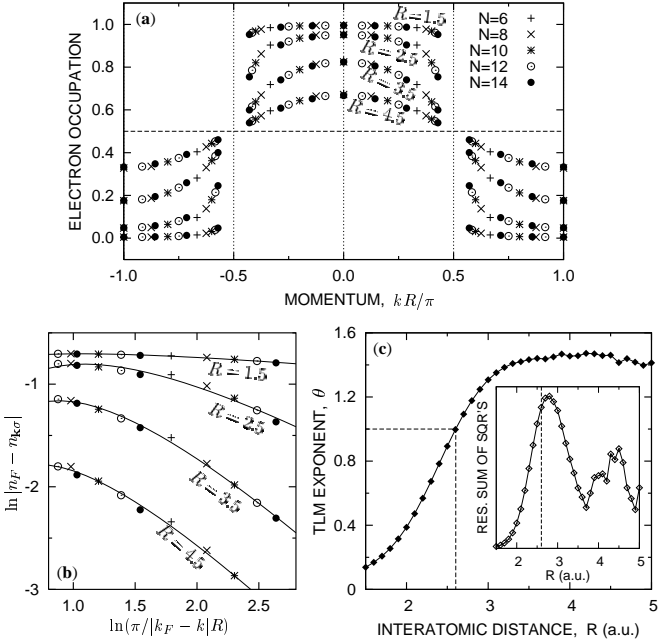


**Fig. 2.** Statistical distribution of electrons and Luttinger–liquid scaling for a half-filled 1D chain of  $N = 6 \div 14$  atoms with long-range Coulomb interactions: (a) momentum distribution for electrons in the linear and (b) log–log scale; (c) Tomonaga–Luttinger model exponent  $\theta$  vs. lattice parameter  $R$  (specified in  $a_0$ ) and (inset) the corresponding residual sum of squares. Solid lines in Figs. (a) and (b) represent the fitting of Eq. (3).

radius). We also give the *residual sum of squares* (cf. inset in Fig. 2c), which shows that the quality of the fit becomes worst for  $R \approx R_c$  where the system approaches the localization threshold.

The results for the half-filled system with the *on-site* Hubbard repulsion alone, and with the atomic energy part included explicitly as a function of  $R$  [13], are qualitatively very similar to those displayed in Fig. 2. The critical value of the lattice parameter in this case is  $R_c = 2.16a_0$ , and does not differ drastically from the previous one (cf. Table 3 for the corresponding values of all the fitted parameters in the Hubbard–model case). This is because such nanoscopic systems always have a finite conductivity in the large–density limit, since electrons tunnel through a finite–width and finite–height potential barrier. Therefore, such half-filled systems, both with and without inclusion of the long–range interactions, can be considered as being close to the metal–insulator transition, in no apparent contradiction with the infinite–chain RG result by Fabrizio [14], and the Hubbard–model solution by Lieb and Wu [15], which both provide only the Mott insulating behavior. This discussion is complete only after calculating the charge and spin gaps, as well as the electric conductivity, which are dealt with in the next two Sections.

The present analysis supplements the earlier discussion [5,7,10], in which we have interpreted the distribution  $n_{k\sigma}$  in Fig. 2a in terms of the modified Fermi distribution for an *almost localized* Fermi liquid. The points

**Table 2.** The parameters of the expansion (3) for the half-filled chain with long-range Coulomb interactions. The corresponding standard deviations  $\sigma(X)$  for the quantities  $X = \theta, b$  and  $c$  are also specified.

$R/a_0$	$\theta$	$\sigma(\theta)$	$b$	$\sigma(b)$	$c$	$\sigma(c)$
1.5	0.138	0.015	0.147	0.024	-0.567	0.015
2.0	0.387	0.055	0.425	0.089	-0.346	0.053
2.5	0.893	0.122	0.971	0.196	0.084	0.118
3.0	1.307	0.128	1.315	0.207	0.357	0.125
4.0	1.455	0.186	1.113	0.299	-0.032	0.180
5.0	1.413	0.133	0.943	0.214	-0.823	0.129

**Table 3.** The fitted parameters of the singular expansion (3) for a half-filled 1D Hubbard chain.

$R/a_0$	$\theta$	$\sigma(\theta)$	$b$	$\sigma(b)$	$c$	$\sigma(c)$
1.5	0.229	0.030	0.237	0.048	-0.537	0.029
2.0	0.803	0.100	0.855	0.162	-0.078	0.097
2.5	1.283	0.109	1.259	0.176	0.217	0.106
3.0	1.420	0.075	1.230	0.121	0.116	0.073
4.0	1.436	0.069	1.033	0.111	-0.456	0.067
5.0	1.371	0.037	0.873	0.060	-1.218	0.036

are arranged in an almost flat manner for the interatomic distance  $R = 1.5a_0$ , suggesting that some kind of quasi-discontinuity of  $n_{k\sigma}$  exists near  $k_F$ . However, an ambiguity arises because of the circumstance that for nanosystems, the points very close to the Fermi momentum for  $N \rightarrow \infty$  system, i.e. the point  $k_F^\infty = \pi/(2R)$ , are simply missing. Nonetheless, it is amazing that the momentum distribution can be rationalized in such simple terms (as either the Fermi or the Tomonaga–Luttinger liquids), which represent concepts borrowed from the  $N \rightarrow \infty$  limit. One should also say that the critical value of  $R_c = 2.60a_0$  for the localization of the single–particle states obtained here is about 30% lower than the corresponding value  $R_c = 3.93a_0$  obtained when we treat the distribution  $n_{k\sigma}$  as the modified Fermi distribution. However, a discrepancy of this order should not be surprising anybody, since the localization criteria should be treated as semi-quantitative at best. One can hope to clarify the situation by extending the present analysis to larger  $N$ . Nevertheless, if we regard a nanoscopic system of  $N \sim 10$  atoms as a *real systems*, then the ambiguity of the statistical distribution is significant. Also, the *partial localization* of electrons in a nanosystem will become apparent when we discuss the multiparticle wave–function localization at the end of this Section, and the conductivity in the *next* Section.

We allow ourselves one specific suggestion (if not speculation) at this point. Namely, the results shown in Fig. 2 (and the discussion in the remaining part of the paper) point to the possibility that the system with small  $R \lesssim 2a_0$  can be analyzed as a Landau–Fermi liquid (albeit with discrete momentum states [16]), whereas the system with  $2a_0 \lesssim R \lesssim 2.5a_0$  is closer to the Tomonaga–Luttinger–Solyom limit. For  $R \gtrsim 2.5a_0$  the electrons can be regarded as effectively localized. Such a division into *three physically*

*distinct* regimes requires a further discussion, carried out, to some extent, below.

Finally, it should be noted that a well-defined spin-spin correlations of the *spin-density-wave* type develop with the increasing  $R$  for the half-filled case, as discussed elsewhere [7,13]. The system ground-state energy as a function of  $R$  is also provided there.

### 3.2 Onset of the charge-density wave state for the quarter filling

The electron quasi-momentum distribution for the *quarter-filled* (QF) case ( $N_e = N/2$ ) is shown in Fig. 3. The available number of data points is too small to fit the singular formula (3) to a reasonable accuracy. In effect, the lines on the plots are a guide for the eye. However, the smooth behavior of the Luttinger-liquid type is evident for  $R \lesssim 4a_0$ , and changes dramatically for the larger values of  $R$ . This change reflects the onset of the *charge-density-wave ordering*, as illustrated in Fig. 4. In a QF chain of  $N = 16$  atoms (*cf.* Fig. 4a) the charge is almost uniformly distributed for  $R \lesssim 3a_0$ , but the charge

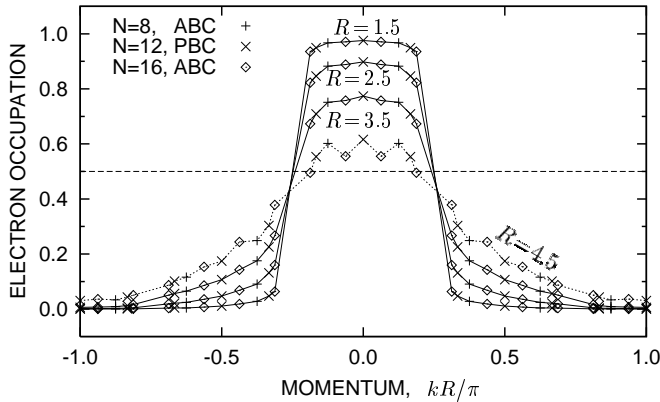


**Fig. 3.** Momentum distribution  $n_{k\sigma}$  for electrons on a chain of  $N = 8 \div 16$  atoms in the *quarter-filled* case ( $N_e = N/2$ ). Lines are drawn as a guide to the eye only. ABC and PBC denote the *antiperiodic* and *periodic* boundary conditions.

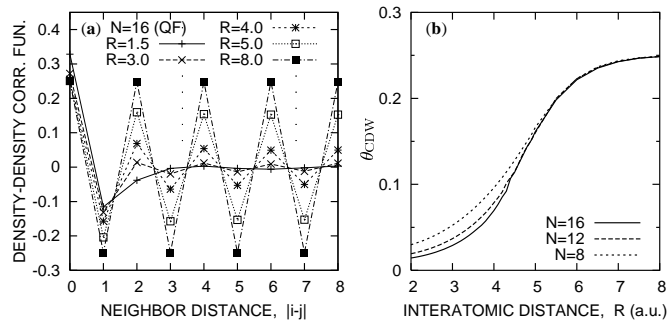


**Fig. 4.** Charge-density distribution for the *quarter-filled* ( $N_e = N/2$ ) nanochain: (a) density fluctuation correlation function  $\langle \Delta n_i \Delta n_j \rangle$  vs. distance  $|i - j|$ , (b) *charge-density wave* order parameter for the density-density fluctuation (*see* main text for the definition) vs. interatomic distance  $R$ .

wave (CDW) sets in very rapidly in the range  $R/a_0 = 4 \div 5$ . The CDW order parameter, defined as  $\theta_{CDW} \equiv N^{-1} \sum_m (-1)^m \langle \Delta n_i \Delta n_{i+m} \rangle$ , (where  $\Delta n_i \equiv n_i - \langle n \rangle$ ) approaches its maximal value  $\theta_{CDW} = 1/4$  for  $R \gtrsim 8a_0$  (*cf.* Fig. 4b). Also, the crossover range of  $R$ , where  $\theta_{CDW}$  evolves from  $\theta_{CDW} \approx 0$  to the perfect-order value  $\theta_{CDW} = 1/4$ , shrinks systematically with the increasing  $N$ , suggesting *quantum critical behavior* in the large- $N$  limit. One can argue that the charge-ordered state for larger  $R$ , corresponding to 1D *Wigner-crystal* state on a lattice, is unstable in the  $N \rightarrow \infty$  limit, in accordance with the Mermin–Wagner theorem. Namely, we expect the amplitude of the quantum charge fluctuations to diverge at zero temperature as  $\log N$  for the system with a long-range ( $\sim 1/r$ ) Coulomb coupling. However, the divergence is absent for  $R \gtrsim 5a_0$  in the exact-diagonalization data for  $N = 8 \div 16$  (*cf.* Fig. 4b), indicating that the zero-point charge fluctuations are suppressed by the onset of the CDW state. In other words, the larger lattice parameter  $R$ , the larger the system which can be regarded as charge ordered in the quarter-filled case. This notion agrees with the expected atomic-limit charge-order in the QF case. The correspondence between the appearance of such charge order and the system conductivity is discussed in the *next* Section, but first, we supplement our analysis of the system ground-state properties with the many-body wavefunction localization in the framework proposed by Resta [9].

### 3.3 Ground-state wavefunction localization

The approach [9] to the electron localization in the correlated state is based on the idea that, although the insulating or the metallic states of matter are usually characterized by their excitation spectrum, the qualitative difference in *dc* conductivity must also reflect a qualitative difference in the organization of electrons in their ground state. Such a concept was first emphasized by Kohn in a milestone paper [17], but a complete treatment, related to the Berry-phase theory of polarization, was proposed over 30 years later by Resta and Sorella (*cf.* Ref. [18]). In their approach the complex number

$$z_{N_e} = \langle \Psi_0 | e^{i(2\pi/L)\hat{X}} | \Psi_0 \rangle \quad (4)$$

(where  $\hat{X}$  is a many-body position operator defined in 1D as  $\hat{X} \equiv \sum_j x_j$  and  $L = NR$  is the system length) is used to discriminate between a localized  $N_e$ -particle ground state (where  $|z_{N_e}| \rightarrow 1$  for large systems) and a delocalized one, where  $z_{N_e}$  vanishes. Namely, the qualitative measure of the electron localization is defined as

$$\langle x^2 \rangle_c = -\frac{1}{N_e} \left( \frac{L}{2\pi} \right)^2 \log |z_{N_e}|^2 = -\frac{NR^2}{4\pi^2 \bar{n}} \log |z_{N_e}|^2 \quad (5)$$

(where  $\bar{n} = N_e/N$  is the average electron density), whereas the phase of the complex number  $z_{N_e}$  is related to the macroscopic system polarization. One should note at this point that the kind of localization described by Eq. (5) is

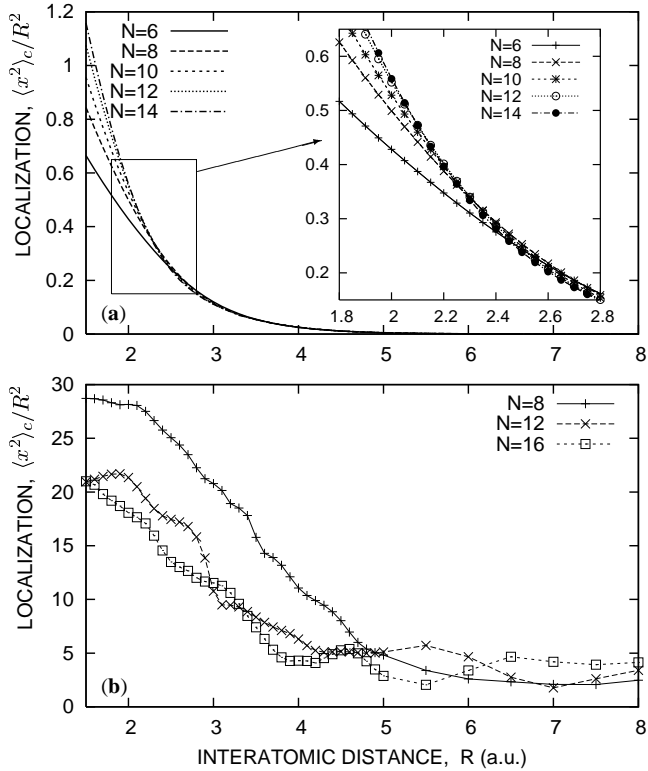


**Fig. 5.** Localization parameter for the ground-state multiparticle wavefunction of the *half-filled* (a) and the *quarter-filled* (b) nanochains. The values of the localization parameter (see main text for the definition) are specified in the units of  $R$ .

clearly *not* a feature characterizing the individual single-particle orbitals; instead, it is a global property of a multiparticle ground-state wavefunction *as a whole*. That is because the operator  $e^{i(2\pi/L)\hat{X}}$  in Eq. (4) *cannot* be expressed as a single-particle operator (like  $\hat{X}$ ) but rather as a *genuine* many-body operator.

The numerical evaluation of the complex number  $z_{N_e}$  and the resulting  $\langle x^2 \rangle_c$  within the Lanczos algorithm is straightforward, since the operator  $e^{i(2\pi/L)\hat{X}}$  in Eq. (4) is diagonal in the position representation. The results for a 1D system with long-range Coulomb interaction are shown in Fig. 5 for both the half- and the quarter-filled cases (*cf.* Fig. 5a and 5b, respectively). To avoid confusion by changing the system length  $L$ , we plot the localization data in units of the lattice parameter  $R$ , namely  $\langle x^2 \rangle_c / R^2$ , instead of  $\langle x^2 \rangle_c$ . The values of the localization parameter, depicted in Fig. 5a, gradually decay with growing  $R$  for all available numbers of atoms  $N$ . However, the dramatic change of the decay character takes place around the value of the lattice parameter  $R \approx 2.5a_0$  (*cf.* *inset* in Fig. 5a), where the curves for different  $N$  join together and form a single one for  $R \gtrsim 2.5a_0$ . In contrast, for lower values of  $R$ , the curves are well separated there by showing the divergence of the localization parameter with  $N$  for  $R \lesssim 2a_0$ . The results for the Hubbard model (not shown) again does not differ qualitatively from those presented in Fig. 5a; the coalescence point is located near the value  $R \approx 2.2a_0$ . The

positions of the joining points for both the models (with and without inclusion of the long-range Coulomb interactions) are very close to the corresponding critical values  $R_c$  obtained from the Tomonaga–Luttinger scaling at the beginning of this Section.

The numerical results for the quarter-filled case, shown in Fig. 5b, are of lesser accuracy than those for the half-filling. This is because the complex expectation value  $z_{N_e}$ , defined by Eq. (4), is itself a sum of many complex numbers with different phases, when calculated in the position representation. If the resulting  $z_{N_e}$  is close to zero, which is the case for QF for all examined values of  $R$ ; it is, in turn, strongly affected by the computer roundoff errors, which are also amplified by taking the logarithm of  $|z_{N_e}|^2$  when calculating  $\langle x^2 \rangle_c$  from Eq. (5). Nevertheless, the evolution of the wavefunction localization parameter versus  $R$  is qualitatively similar to that for the half-filled case: the curves for different system sizes  $N$ , depicted in Fig. 5b, get very close to each other for  $R \gtrsim 4.5a_0$  where the charge-density wave state is formed, as discussed in the preceding subsection.

The apparent correspondence between the wavefunction localization properties and the nature of electron momentum distribution, both discussed in this Section, suggests that a significant reorganization of the ground state takes place when the nanochain is close to the localization threshold. These observations are supplemented in the *next* Section with analysis of the system energy gap, the spectral function, and the transport properties.

## 4 Spectral and transport properties

### 4.1 The charge and spin gaps

For a further verification, of whether the system is quasi-metallic or quasi-insulating in the Luttinger-liquid like regime, we first perform an extrapolation with  $1/N \rightarrow 0$  of the charge-gap defined (for the *half-filling*) as

$$\Delta E_C(N) = E_G^{N+1}(N) + E_G^{N-1}(N) - 2E_G^N(N), \quad (6)$$

where  $E_G^{N_e}(N)$  is the ground-state energy of the  $N$ -site system containing  $N_e$  electrons. The corresponding numerical results are shown in Fig. 6, where we use again the proper boundary conditions (*periodic* or *antiperiodic*, depending on  $N$ ) which minimize the ground-state energy. The extrapolation of  $1/N \rightarrow 0$  performed using the 2-nd and the 3-rd order polynomials in  $(1/N)$  provides a nonzero value of  $\Delta E_C$  for wide range of the lattice parameter  $R$ . Only for the lowest examined value of  $R = 1.5a_0$  does the gap  $\Delta E_C$  reaches zero within the extrapolation error; for  $R > 1.5a_0$  it is clearly nonvanishing. The gap is also significantly smaller than the corresponding Hartree–Fock value (*dotted* line) in the regime  $R \lesssim 4.5a_0$ , suggesting that some kind of reorganization is present in the dielectric properties, e.g. a crossover from the Slater- to the Mott-type insulator, as discussed for the parametrized models [18]. This hypothesis is verified by estimating the

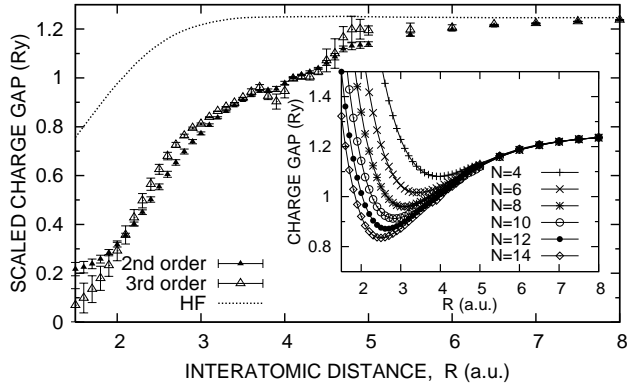


**Fig. 6.** Charge–energy gap obtained through the finite–size scaling of the results for the chains of  $N = 4 \div 14$  atoms. The corresponding Hartree–Fock (HF) value of the magnetic gap for an infinite system is also drawn for comparison (*dotted* line). The *inset* exhibits the original data for different values of  $N$ , used for the scaling. *Note* a qualitative difference between the scaled (with  $1/N \rightarrow 0$ ) and the actual gap values.

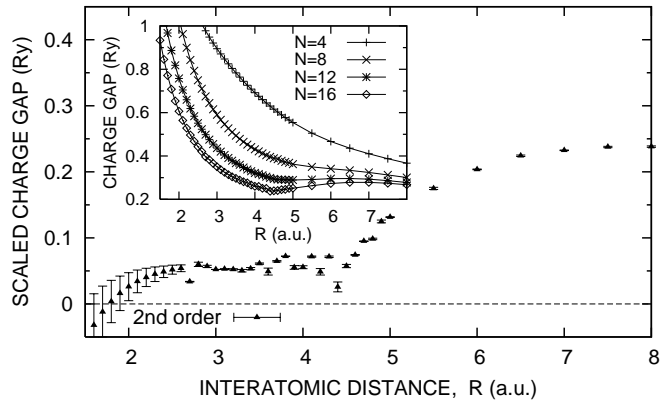


**Fig. 7.** Charge–energy gap obtained through the finite–size scaling of the results for the chains of  $N = 4 \div 16$  atoms in the *quarter-filled* case. The 2–nd order polynomial has been fitted to perform the extrapolation with  $1/N \rightarrow 0$ . *Inset* provides the original data used for the scaling.

spin gap *below*. One should also note a qualitative difference between the behavior of  $\Delta E_C$  for nanoscopic chains (*cf.* the *inset*) and of their  $N \rightarrow \infty$  correspondants. Therefore, the finite– $N$  system contains physically different dynamic properties.

The situation changes when we consider the *quarter-filled* case,  $N_e = N/2$  (*cf.* Fig. 7). The parabolic extrapolation with  $1/N \rightarrow 0$  now provides the value of the charge–gap  $\Delta E_C \approx 0$  (within the error bars) for the lattice parameter  $R \lesssim 2a_0$ . In the range of  $R/a_0 = 2.5 \div 4.5$  the gap develops (it is significantly greater than the corresponding error bars), but a random dispersion of the data points suggests an inaccuracy of the extrapolation due to the nonanalytic behavior of  $\Delta E_C$  when the system approaches the localization threshold. For  $R \gtrsim 4.5a_0$  the gap grows smoothly to a limiting value corresponding to that for the insulating charge–density wave state, identified earlier. The more precise position of the localization

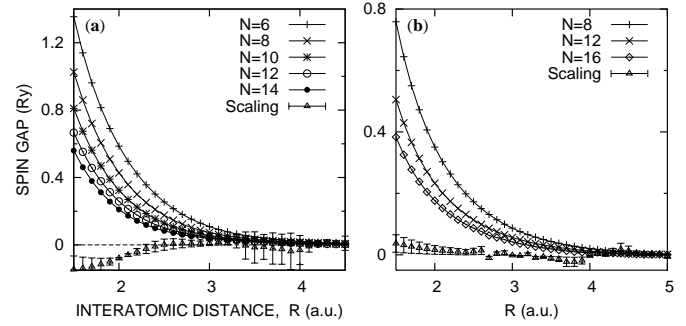


**Fig. 8.** Spin gap for the *half-filled* (a) and the *quarter-filled* (b) nanochains. The results obtained through the finite–size scaling are also shown with the corresponding errorbars.

point is determined later in this Section, where we calculate the system Drude weight.

For the sake of completeness, in Fig. 8 we provide the values of the system *spin gap*, which is defined as

$$\Delta E_S(N) \equiv E_G^{S_z=1}(N) - E_G^{S_z=0}(N), \quad (7)$$

where  $E_G^{S_z}(N)$  denotes the lowest eigenenergy of  $N$ –site system in the subspace with a given total  $z$ –component of spin  $S_z$ . Through the finite–size scaling with  $1/N \rightarrow 0$ , we obtain the spin gap  $\Delta E_S \approx 0$  for both the half– and the quarter–filled cases (*cf.* Figs. 8a and 8b, respectively), and in the whole examined range of the interatomic distance  $R$ . These results clearly show that the insulating phase of the system is of the Mott type in the large– $N$  limit. No indications of the Slater–type phase, for which  $\Delta E_C = \Delta_S > 0$ , was found. However, for a nanosystem containing  $N \sim 10$  atoms, one can note that the so–called *correlated insulator* ( $\Delta E_C > \Delta_S > 0$ ), existing for the small values of  $R$  (*cf.* *insets* to Figs. 6 and 7, and Fig. 8) gradually transforms into the Mott insulator with increasing  $R$ . This evolution should be contrasted with the evolution of bulk 3D systems where the Slater antiferromagnet evolves into the Mott insulator (*cf.* Korbel *et al.*, Ref. [18]).

## 4.2 Spectrum of single–particle excitations: renormalized bands vs. Hubbard subbands

The evolution of the single–particle spectral density function  $A_{\mathbf{k}}(\omega)$  with increasing  $R$  is shown in Fig. 9a for the *half-filled* ( $N_e = N$ ) nanochain described by the Hamiltonian (1). The spectral function is defined in the standard manner, namely

$$A_{\mathbf{k}}(\omega) = \sum_n |\langle \Psi_n^{N\pm 1} | c_{\mathbf{k}\sigma}^\pm | \Psi_0^N \rangle|^2 \delta [\omega - (E_n^{N\pm 1} - E_0^N)], \quad (8)$$

where the upper (lower) sign correspond to  $\omega > \mu$  ( $\omega < \mu$ ), respectively,  $|\Psi_n^N\rangle$  is the  $n$ –th eigenstate of the system containing  $N$  particles,  $E_n^N$  is the corresponding eigenenergy, and the matrix element  $\langle \Psi_n^{N\pm 1} | c_{\mathbf{k}\sigma}^\pm | \Psi_0^N \rangle$ , with  $c_{\mathbf{k}\sigma}^+ \equiv a_{\mathbf{k}\sigma}^\dagger$  and  $c_{\mathbf{k}\sigma}^- \equiv a_{\mathbf{k}\sigma}$ , is calculated within the Lanczos technique set up by Dagotto [20]. For plotting purposes, we

have used the analytical representation of the Dirac delta function  $\delta(x) \rightarrow (1/\pi)\epsilon/(x^2 + \epsilon^2)$  with  $\epsilon = 0.01$  Ry; this numerical trick leads to peaks with nonzero width, which otherwise would be discrete. In the nanometallic range ( $R \lesssim 2.5a_0$ ), the quasiparticle peaks are well defined, but incoherent tails are always present and grow in strength with increasing  $R$ . In effect, in the intermediate regime of  $R \sim 3a_0$  the lower and upper Hubbard bands are formed, which, in turn, continuously evolve into discrete atomic levels located at the positions  $\omega = \epsilon_a$  and  $\omega = \epsilon_a + U$ , when  $R \rightarrow \infty$  (cf. Fig. 9d). These limiting peak positions correspond to the ground ( $H^0$ ) and excited ( $H^-$ ) atomic levels. Possibly the most interesting feature of this spectrum is its *incoherent* nature for  $R \sim 3a_0$ , where the band and the interaction energies are comparable and where the Luttinger liquid exponent crosses the critical value  $\theta = 1$  (cf. Section 3.1), corresponding to the localization threshold.

A direct picture of the spectrum evolution is provided by the *renormalized* dispersion relation, which is obtained from the spectral function by extracting the major quasiparticle peak position for each momentum  $k$ , and is plotted in Figs. 9b–d. We can again easily identify: (i) the *nanometallic range* (cf. Fig. 9b for  $R = 1.5a_0$ ), for which the charge gap is of the same order as the energy discretization due to the geometrical quantization of the quasiparticle momenta, (ii) the *intermediate regime* (cf. Fig. 9c,  $R = 3a_0$ ) where the gap becomes significantly wider, and (iii) the *atomic limit* (cf. Fig. 9d,  $R = 8a_0$ ) in which two dispersionless manifolds located at energies  $\omega = \epsilon_a$  and  $\omega = \epsilon_a + U$  appear. One should also note that the corresponding results for the antiferromagnetic Hartree–Fock solution (*solid lines*) closely match

those obtained within the EDABI method, both for the *atomic* and for the *nanometallic* limits (particularly for the upper Hubbard band in the latter case). The electron–correlation effects, in contrast, clearly appear (near the Fermi momenta) for the intermediate range of  $R$ , where the Hartree–Fock charge gap is significantly larger than the exact one (cf. also the *preceding* Section). Another interesting feature of the renormalized dispersion relation is that the datapoints for different  $N$  ( $= 10$  and  $12$ ) compose a single (*universal*) renormalized band–like dispersion relation  $\tilde{\epsilon}_{\mathbf{k}}$ , provided that the proper boundary conditions which minimize the ground–state energy for a particular  $N$  are applied.

The results for the renormalized band energy  $\tilde{\epsilon}_{\mathbf{k}}$ , together with those for the distribution function  $n_{\mathbf{k}\sigma}$  (cf. Fig. 2a), characterize in a *fundamental manner* the salient features of the electronic states for the *quantum nanoliquid*. Also note, that the gap in the single–particle spectrum is always present, that is partially caused by the absence of the  $k$  states near the Fermi point  $k_F^\infty$ , and partially by the electron–electron interaction. The role of the geometrical momentum quantization is dominant in the large–density limit ( $R \lesssim 2a_0$ , cf. Fig. 9b), whereas the Coulomb repulsion determines the single–particle gap in the large– $R$  limit (cf. Fig. 9d). What is remarkable at this point, is that the Hartree–Fock approximation works well in both limits of weak and strong electron correlations mentioned above, but fails in the intermediate range ( $R \sim 3a_0$ , cf. Fig. 9c). One also can say that we observe a magnetic (Slater) gap contribution to the renormalized band structure of nanoscopic system even though we only observe SDW–like correlations, but *no* spontaneous symmetry breaking. This is another *fundamental feature* of these systems. The above results will now be supplemented with the transport properties, which are considered next.

### 4.3 Drude weight and optical conductivity

The real part of the optical conductivity at zero temperature is determined by the corresponding real part of the linear response to the applied electric field [19], and can be written as  $\sigma(\omega) = D\delta(\omega) + \sigma_{\text{reg}}(\omega)$ , where the regular part is

$$\sigma_{\text{reg}}(\omega) = \frac{\pi}{N} \sum_{n \neq 0} \frac{|\langle \Psi_n | j_p | \Psi_0 \rangle|^2}{E_n - E_0} \delta(\omega - (E_n - E_0)), \quad (9)$$

whereas the Drude weight (the *charge stiffness*)  $D$  is defined by

$$D = -\frac{\pi}{N} \langle \Psi_0 | T | \Psi_0 \rangle - \frac{2\pi}{N} \sum_{n \neq 0} \frac{|\langle \Psi_n | j_p | \Psi_0 \rangle|^2}{E_n - E_0}, \quad (10)$$

where the kinetic–energy term  $T$  is the same as the second term in Eq. (1), and the diamagnetic current operator defined as usual:  $j_p = it \sum_{j\sigma} (a_{j\sigma}^\dagger a_{j+1\sigma} - \text{HC})$ . Here the states  $|\Psi_n\rangle$  in Eqs. (9) and (10) are the eigenstates

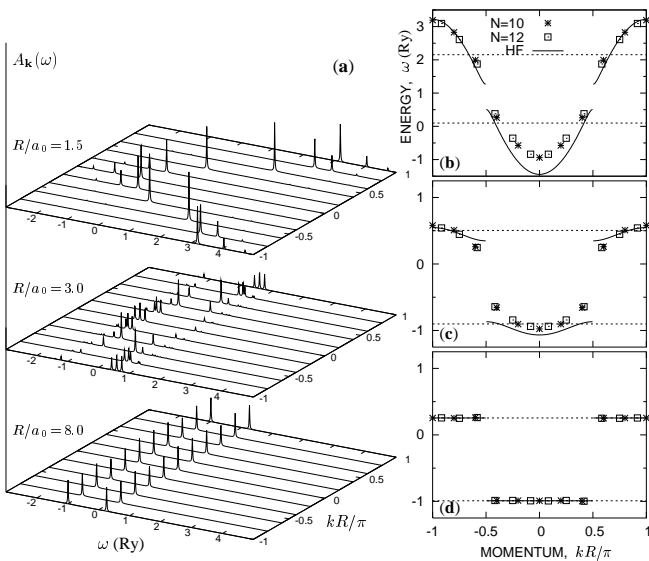


**Fig. 9.** Spectral functions  $A_{\mathbf{k}}(\omega)$  for the nanochain of  $N = 10$  atoms (a) and the corresponding renormalized dispersion relations (band energies with a gap) for the lattice parameter  $R = 1.5a_0$  (b),  $R = 3a_0$  (c), and  $R = 8a_0$  (d). The quasiparticle energies for *antiferromagnetic* Hartree–Fock solution (*solid lines*) are also shown for the comparison.



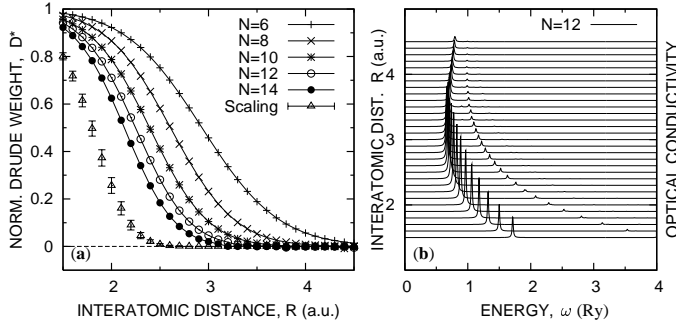


**Fig. 10.** Optical conductivity for nanochains in the *half-filled* case: (a) normalized Drude weight vs. lattice parameter  $R$  (specified in  $a_0$ ) and its values obtained through the finite size scaling ( $1/N \rightarrow 0$ ); (b) regular part of the conductivity,  $\sigma_{\text{reg}}(\omega)$  for  $N = 12$  atoms.

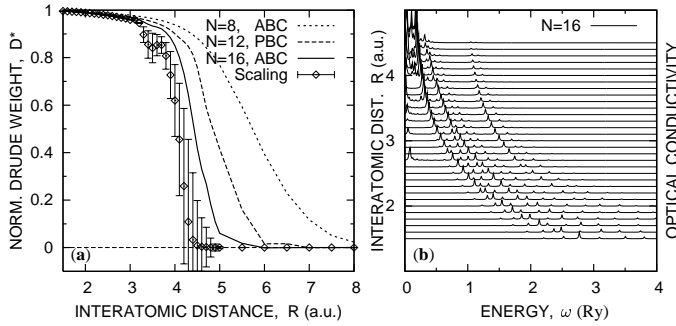


**Fig. 11.** Optical conductivity for the *quarter-filled* chain: (a) normalized Drude weight vs. lattice parameter  $R$  and its values extrapolated to  $1/N \rightarrow 0$  (the Aitken method has been used to estimate the errors); (b) regular part of the conductivity,  $\sigma_{\text{reg}}(\omega)$  for  $N = 16$  atoms.

of the Hamiltonian (1) corresponding to the eigenenergies  $E_n$ , again with boundary conditions which minimize the ground-state energy for a given system size  $N$ . Matrix elements  $\langle \Psi_n | j_p | \Psi_0 \rangle$  are calculated within the Lanczos method [20]. For plotting purposes, we also again use the analytic representation of Dirac delta function  $\delta(x) \rightarrow (1/\pi)\epsilon/(x^2 + \epsilon^2)$ , with  $\epsilon = 0.01$  Ry.

For a finite system of  $N$  atoms,  $D$  is always nonzero due to a nonzero tunneling probability through a potential barrier of finite width. Because of that, the finite-size scaling with  $1/N \rightarrow 0$  has to be performed on  $D$ . Here we use, after Góra *et al.* [21], the following parabolic extrapolation

$$\ln |D_N^*| = a + b(1/N) + c(1/N)^2, \quad (11)$$

where  $D_N^*$  denotes the *normalized Drude weight*  $D^* \equiv -(N/\pi)D / \langle \Psi_0 | T | \Psi_0 \rangle$  for the system of  $N$  sites, which provides the value in the range  $0 \leq D^* \leq 1$ , and thus can be regarded as an alternative order parameter for the transition to the localized (atomic) state.

The results for the 1D system of  $N = 6 \div 14$  atoms in the *half-filled* chain case are shown in Fig. 10a. The values of  $D_N^*$  used for the scaling (11) are listed in Table 4, together with the resulting  $D_\infty^*$  and its relative error (we stop at the lattice parameter  $R$  for which  $D_\infty^* = 0$ ,

within the range of errorbars). We also provide, for comparative purposes, the data for the system with the *on-site* Coulomb interaction only (i.e. for the Hubbard model) in Table 5. In both cases, i.e. that with the long-range interactions (*cf.* Table 4), and that with the on-site interaction only (*cf.* Table 5), the extrapolated Drude weight  $D_\infty^*$  becomes significantly greater than zero (of  $2\sigma$  value) only for small lattice parameter, i.e. for  $R \leq 2.6a_0$  and  $R \leq 2.1a_0$ , respectively. The limiting values match well those for which the Luttinger–liquid exponent crosses the critical value  $\theta = 1$ , corresponding to the localization–delocalization boundary. The above results suggest again the localization onset in these 1D systems at half-filling. However, the optical conductivity  $\sigma_{\text{reg}}(\omega)$ , drawn in Fig. 10b, shows the isolated Hubbard peak at  $\omega \approx U$  and *no intraband transitions* present in the delocalized state. Because of this fact, and also because of the nonzero value of the charge-gap for any  $R$  (*cf. above*), one should regard both the half-filled systems studied here as the Mott insulators in the large  $N$  limit. Nevertheless, the finite- $N$  results show that the conductivity of the nanoscopic chain diminishes by two orders of magnitude when the corresponding increase of the lattice parameter  $R$  is in the range of  $40 \div 50\%$ . So, one can consider such system as undergoing a transformation either from a *nanoliquid* to the *localized spin system* at the half-filling or from an intrinsically *partially localized* state, since the intraband transitions are absent even in the small- $R$  range. It would be very interesting to confirm these results experimentally.

The situation again becomes completely different at the *quarter-filling* (QF). Namely, the normalized Drude weight of the QF systems of  $N = 8 \div 16$  atoms, depicted in Fig. 11a, shows a *highly-conducting* behavior ( $D^* \approx 1$ ) for  $R \lesssim 3.5a_0$ , and gradually transforms to zero in the range  $R/a_0 = 4 \div 5$ . Also, the regular part of the conductivity  $\sigma_{\text{reg}}(\omega)$  (*cf.* Fig. 11b) comprises intraband transitions in the quasi-metallic range, particularly near the onset of the charge-density wave state (for  $N = 16$ ). Such a behavior provides the model case for the transformation from a nanometal in the small- $R$  range to the charge-ordered system (*cf.* Fig. 4) for larger  $R$ .

## 5 A brief overview: Novel features

We have provided a fairly complete description of the electronic states in a finite 1D chain within the framework of the EDABI method, which combines the *exact diagonalization* of the many-fermion Hamiltonian in the Fock space with a subsequent *ab initio* readjustment of the single-particle (Wannier) functions. Both the ground-state and dynamical properties have been obtained as a function of the variable lattice parameter (interatomic spacing)  $R$ . Our approach thus *extends* the current theoretical treatments of band and strongly correlated systems within the parametrized (second-quantized) models, by determining those parameters and, in turn, analyzing the correlated state explicitly as a function of  $R$ . The single-particle wave function is allowed to readjust in the correlated state within the EDABI method, thus unifying the

**Table 4.** Normalized Drude weight  $D_N^*$ , the extrapolated value  $D_\infty^*$ , and its relative error for 1D half–filled system with long–range Coulomb interaction. The critical value  $R_c \approx 2.6a_0$  is determined from the condition  $D_\infty^* = 2\sigma(D_\infty^*)$ .

$R/a_0$	$D_{14}^*$	$D_{12}^*$	$D_{10}^*$	$D_8^*$	$D_6^*$	$D_\infty^*$	$\sigma(D_\infty^*)/D_\infty^*$
1.5	0.9225	0.9420	0.9563	0.9727	0.9822	0.8008	0.019
2.0	0.6245	0.7105	0.7875	0.8660	0.9222	0.2567	0.129
2.5	0.1839	0.2812	0.4109	0.5813	0.7526	0.0087	0.420
2.6	0.1269	0.2096	0.3315	0.5065	0.7009	0.0033	0.489
2.7	0.0840	0.1508	0.2595	0.4312	0.6441	0.0012	0.566
2.8	0.0536	0.1049	0.1972	0.3586	0.5836	0.0004	0.641
2.9	0.0315	0.0706	0.1456	0.2914	0.5208	0.0001	0.920
3.0	0.0196	0.0461	0.1047	0.2314	0.4575	0.0000	–

**Table 5.** Normalized Drude weight  $D_N^*$ , the extrapolated value  $D_\infty^*$ , and its relative error for 1D half–filled system described by the Hubbard model. The critical value  $R_c \approx 2.1a_0$  is determined as for the long–range interaction case (*cf.* Table 4).

$R/a_0$	$D_{14}^*$	$D_{12}^*$	$D_{10}^*$	$D_8^*$	$D_6^*$	$D_\infty^*$	$\sigma(D_\infty^*)/D_\infty^*$
1.5	0.6173	0.6742	0.7342	0.7973	0.8640	0.3294	0.070
2.0	0.1529	0.2259	0.3276	0.4631	0.6331	0.0092	0.364
2.1	0.0991	0.1598	0.2527	0.3884	0.5731	0.0032	0.449
2.2	0.0619	0.1094	0.1896	0.3190	0.5123	0.0010	0.540
2.3	0.0372	0.0724	0.1382	0.2561	0.4514	0.0003	0.639
2.4	0.0218	0.0467	0.0985	0.2018	0.3927	0.0001	0.739
2.5	0.0124	0.0294	0.0687	0.1561	0.3372	0.0000	–

second and the first quantization aspects of the many–particle states into a single, *fully microscopic* scheme.

We start by analyzing the situation with one valence electron per atom (the *half–filled* case), and we include the *long–range* Coulomb interaction. The Luttinger–liquid type of electron momentum distribution suggests a *crossover transition* from the quasi–metallic to the insulating (*spin–ordered*) state with increasing  $R$  (the same is true about the system without the long–range interaction [13], but the quasi–metallic behavior is manifested to a much stronger degree when the long–range part of the Coulomb interactions is included). The finite–size scaling with  $(1/N \rightarrow 0)$ , performed on the charge–energy gap shows the insulating nature of the ground state for the large  $N$  limit, in agreement with the renormalization–group results for the *infinite* system with two Fermi points [14]. Such an apparently dichotomic nature (localized vs. itinerant) of the nanoscopic systems is confirmed by their transport properties. On the one hand, the Drude weight is nonzero in the small  $R$  limit, and the localization threshold agrees with those obtained from the Luttinger–liquid exponent, but the regular part of the optical conductivity exhibits the insulating behavior. This is the reason we coined the term: *a partially localized quantum nanoliquid*. The most fundamental features of the electrons as a *quantum nanoliquid* is provided in Figs. 2a and 9b–d, where the *Fermi–like* distribution, as well as the *renormalized band structure* appear for small interatomic spacing. These features evolve with  $R \rightarrow R_c$  into *atomic–like* through the regime with split *Hubbard–like* subbands.

An illustrative example of the nanoscopic system with a clear transformation from *nanometal* to *nanoinsulator* with the charge–density wave order is provided with the *quarter–filled* nanochain (including again the long–range Coulomb interaction). For that system, the Drude weight is reduced gradually from its maximal value to zero, and other properties evolve analogously with increasing lattice parameter  $R$ . The intermediate range of  $R$ , where the crossover takes place, also shrinks rapidly with increasing  $N$ , suggesting the existence of a sharp zero–temperature transition in the large  $N$  limit.

The above analysis, for both the half– and the quarter–filled cases is very sensitive to the choice of boundary conditions. This problem is widely studied in the existing literature and its relation to the spontaneous magnetic flux appearing in the mesoscopic rings of  $N = 4n$  atoms [22] has been established before [23].

The EDABI method implemented here can also be applied to discuss the coupling of electrons to the lattice and the dimerization (for a discussion, see the third paper in Ref. [5]). Also, one should incorporate the properties of the chain with an odd number of electrons (the boundary conditions will then involve the complex number domain). Furthermore, the dynamics with single holes and impurities in the nanochain would make the system more realistic as a quantum wire. Finally, the application of the present scheme to higher (*ns–like*) valence orbital systems would make possible a direct comparison with experimental results on quantum nanowires made of noble and alkaline elements. Nonetheless, we believe that our present analysis models the fundamental features of such *quantum*

*nanowires*, particularly their quantum–nanoliquid aspects (evolving Fermi–like distribution, renormalized bands with a gap even in the absence of a long–range order). We should be able to see a progress along these lines soon.

## Acknowledgement

We thank our colleagues: Dr. Maciej Maška and Prof. Krzysztof Rościszewski, for discussions about the Lanczos algorithm and the role of boundary conditions for finite systems. We are also grateful to the Institute of Physics of the Jagiellonian University for the support for computing facilities used in part of the numerical analysis. The support from the Committee for Scientific Research (KBN) of Poland (Grant No. 2P03B 050 23), and from the Polish Foundation for Science (FNP), is acknowledged. The authors are also grateful to one of the Referee whose suggestions improved substantially the paper presentation. With this paper we would like to mark the European Union enlargement on May 1, 2004.

## References

1. P.C. Hohenberg, W. Kohn, L.I. Sham, in *Adv. Quantum Chemistry*, edited by S.B. Trickey, vol. 21 (Academic, San Diego, 1990), p. 7; W. Temmerman *et al.*, in *Electronic Density Functional Theory: Recent Progress and New Directions*, edited by J.F. Dobson *et al.* (Plenum, New York, 1998), p. 327
2. V.I. Anisimov *et al.*, Phys. Rev. B **44**, 943 (1991); P. Wei and Z.Q. Qi, *ibid.* **49**, 10864 (1994)
3. A. Svane and O. Gunnarson, Europhys. Lett. **7**, 171 (1988); Phys. Rev. Lett. **65**, 1148 (1990)
4. S. Ezhov *et al.*, Phys. Rev. Lett. **83**, 4136 (1999); K. Held *et al.*, *ibid.* **86**, 5345 (2001)
5. J. Spalek *et al.* Phys. Rev. B **61**, 15676 (2001), and unpublished; A. Rycerz and J. Spalek, *ibid.* **63**, 073101 (2001); *ibid.* **65**, 035110 (2002); J. Spalek and A. Rycerz, *ibid.* **64**, R161105 (2001)
6. J. Spalek *et al.*, Acta Phys. Polon. B **31**, 2879 (2000); *ibid.* **32**, 3189 (2001)
7. A. Rycerz *et al.*, in *Lectures on the Physics of Highly Correlated Electron Systems VI*, edited by F. Mancini, AIP Conf. Proc. vol. 629 (New York, 2002) p. 213; *ibid.* vol. 678 (New York, 2003) p. 313
8. J. Spalek *et al.*, in *Concepts in Electron Correlation*, Proc. NATO Adv. Res. Workshop, edited by A.C. Hewson and V. Zlatić (Kluwer, Dordrecht, 2003) p. 257; see also: E. Gölich *et al.*, in *Molecular Nanowires and other Quantum Objects*, Proc. NATO Adv. Res. Workshop (Kluwer, Dordrecht, 2003), in press, *cond-mat/0403106*.
9. R. Resta, J. Phys. Condensed Matter **14**, R625 (2002); Phys. Rev. Lett. **80**, 1800 (1998); see also Resta and Sorella, Ref. [18]
10. A. Rycerz *et al.*, Acta Phys. Polon. B **34**, 651 (2003); *ibid.* 655 (2003)
11. J. Solyom, Adv. Phys. **28**, 201 (1979); J. Voit, Rep. Prog. Phys. **57** 977 (1995)
12. S. Sorella *et al.*, Europhys. Lett. **12**, 721 (1990)
13. A. Rycerz, Ph.D. Thesis, Jagiellonian University, Kraków, 2003
14. M. Fabrizio, Phys. Rev. B **54**, 10054 (1996); see also Voit, Ref. [11]
15. E.H. Lieb and F.Y. Wu Phys. Rev. Lett. **20**, 1445 (1968)
16. E.L. Altshuler *et al.*, Phys. Rev. Lett. **78**, 2803 (1997)
17. W. Kohn, Phys. Rev. **133**, A171 (1964)
18. R. Resta and S. Sorella, Phys. Rev. Lett. **82**, 370 (1999); P. Korbel *et al.*, Eur. Phys. J. B **32**, 315 (2003)
19. B.S. Shastry and B. Sutherland Phys. Rev. Lett. **65**, 243 (1990); J.A. Millis and S.N. Coppersmith, Phys. Rev. B **42**, 10807 (1990)
20. E. Dagotto, Rev. Mod. Phys. **66**, 763 (1994); P. Prelovšek and X. Zotos, in *Lectures on the Physics of Highly Correlated Electron Systems VI*, edited by F. Mancini, AIP Conf. Proc. vol 629 (New York, 2002) p. 161
21. D. Góra, K. Rościszewski, A.M. Oleś, J. Phys. Condensed Matter **10**, 4755 (1998)
22. M. Büttiker *et al.*, Phys. Lett. **96A**, 365 (1983); R. Landauer and M. Büttiker, Phys. Rev. Lett. **54** 2049 (1985); D. Mailly *et al.*, *ibid.* **70**, 2020 (1993)
23. M. Abraham, R. Berkovitz, Phys. Rev. Lett. **70**, 1509 (1993); G. Bouzerar, Phys. Rev. B **49**, 8258 (1994); J.–X. Zhu, Z.D. Wang, *ibid.* **52**, 14505 (1995)